It's about time: novel drug discovery concepts for the molecular pharmacological characterization fo the cannabinoid CB2 receptor

Bouma, J.

Chapter 6

Impact of cancer-associated mutations on receptor function and drug targeting of cannabinoid CB_2 receptor

Jara Bouma, Xuesong Wang, Ikram el Miloudi, Silke Cornelissen, Marina Gorostiola González, Antonius P.A. Janssen, Mario van der Stelt, Laura H. Heitman

Abstract

Cannabinoid CB_2 receptor (CB_2R) activation has shown beneficial effects as a potential anticancer treatment strategy. Nevertheless, mutations in CB_2R are found in patient-derived tumor samples, which might affect the protective effects mediated via CB_2R. Therefore, we aimed to investigate the effect of cancer-associated CB_2R mutations on endocannabinoid binding and activation, as well as the druggability of these mutant receptors. To this end, receptor expression of ten mutant CB_2Rs was assessed in an ELISA, followed by a G protein activation screen with an inverse agonist as tool compound to assess receptor state, i.e., basal activity. Furthermore, G protein activation by endogenous and synthetic reference or clinical agonists was assessed and radioligand binding assays were executed to investigate the impact on binding of the radioligand, an endogenous agonist and two clinical agonists. Expression levels of receptors with mutations in the transmembrane domains were similar to wild type (WT), whereas mutations in the flexible regions altered expression levels and receptor state. Furthermore, mutations in the binding pocket and structurally close to a conserved motif markedly affected receptor activation, while mutations in the N- and C-termini were less likely to alter activation. Radioligand binding was reduced for the majority of mutant CB_2Rs. Affinity of the other agonists was only moderately affected on mutant receptors $N11^{N\text{-}term}K$, $D24^{N\text{-}term}N$, $A282^{7.36}T$ and $P348^{C\text{-}term}S$. Overall, our results indicate that cancer-associated mutations in CB_2R can impact the expression, agonist binding and activation of the receptor. This highlights the importance of precision medicine and patient genome screening prior to administration of cannabinoid-based therapies.

6.1 Introduction

Cancer is an extraordinarily complex disease due to the diversity in cancer genotypes and phenotypes[1]. A large cancer genome mutation analysis revealed that in 20% of all human cancers G protein-coupled receptors (GPCRs) were found to be mutated and specific conserved motifs were more prone to mutations[2–4]. Furthermore, GPCRs are involved in cancer-relevant signaling pathways and are therefore hypothesized to be interesting targets for anticancer drugs[5,6]. Nevertheless, the effect of GPCR mutations on cancer progression or druggability is largely unknown[2,5]. Previous studies on cancer-associated mutations for adenosine A_1, A_{2A} and A_{2B} receptors, as well as CC chemokine receptor 2 (CCR2) showed the impact of such mutations on receptor functionality and druggability, underlining the importance to study them[7–11]. Moreover, a recent large investigation on GPCR mutations from patient-derived cancer samples revealed novel GPCRs implicated in cancer development, including the cannabinoid CB_2 receptor (CB_2R)[3].

CB_2R is part of the endocannabinoid system (ECS) along with the cannabinoid CB_1 receptor (CB_1R), the endocannabinoids 2-arachidonoylglycerol (2-AG) and anandamide (AEA), and their metabolizing enzymes[12]. CB_2R is primarily located on immune cells and as such is involved in the regulation of inflammatory processes[13,14]. Nevertheless, dysregulation or altered expression levels of CB_2R have been described for a variety of diseases, including cancer[15,16]. In various cancer types, such as gliomas, human epidermal growth factor 2 (HER2) positive breast tumors and non-small-cell lung cancer, elevated CB_2R levels have been reported[17–20]. It was shown that these increased levels were correlated with a poor patient prognosis and tumor malignancy, as well as a higher probability to develop metastases. Moreover, endogenous CB_2R expression has also been shown to suppress colon tumorigenesis[21].

Nevertheless, this also provides the opportunity to therapeutically exploit CB_2R, which is substantiated by previously described antitumor effects of cannabinoids that have been extensively reviewed[22–25]. The protective effects of cannabinoids via CB_2R activation are regulated through a large variety of pathways and proteins. In HER2 positive breast cancer, non-selective cannabinoid Δ^9-tetrahydrocannabinol (Δ^9-THC) disrupted the heteromerization of HER2 with CB_2R, which consequently triggered antitumor responses in both *in vitro* and *in vivo* models[19]. Moreover, Δ^9-THC has been shown to downregulate matrix metalloproteinase-2 expression in gliomas, which in turn inhibited glioma cell invasion[26]. These effects were mimicked by CB_2R selective agonist JWH133 to further support the protective effect via CB_2R activation[26]. The antitumor effects of JWH133 have been further described in various cancer types, including breast, colon, lung, brain, and skin cancer by inhibition of tumor cell proliferation and migration as well as attenuation of angiogenesis[18,25,27]. Similarly, WIN55,212-2 has been reported to inhibit growth of malignant skin tumor cells and increased the number of apoptotic cells, while impairing tumor vascularization[28]. Recently, a phase II trial with Sativex®, an oromucosal spray with Δ^9-THC and cannabidiol (CBD), showed promising results on the overall survival of patients with recurrent glioblastoma and follow-up clinical trails will focus on the improvement of disease outcomes after treatment with Sativex®[29]. However currently, cannabinoid-based therapies are prescribed to cancer patients experiencing chemotherapy-induced nausea and

vomiting (CINV) or cancer-related anorexia as palliative strategies[30]. Hereto, Dronabinol (Δ^9-THC) and Nabilone are approved drugs and ART-27.13 has completed clinical phase I studies for cancer-related anorexia[13].

In view of the therapeutic potential of CB_2R agonists and the CB_2R mutations found in cancer patient samples, we aimed to investigate the impact of CB_2R cancer-associated mutations on the functionality of the receptors as well as the implications for drug targeting. CB_2R mutations from the Genomic Data Commons (GDC) were collected and narrowed down based on occurrence and proximity to the orthosteric binding pocket. Expression and G protein activation on ten mutant CB_2Rs was investigated by screening a variety of CB_2R ligands in [^{35}S]GTPγS assays. The endocannabinoids 2-AG and AEA were screened to investigate the endogenous implications of mutant CB_2Rs (**Figure 6.1**). Furthermore, structurally diverse reference agonists CP55,940, WIN55,212-2 and JWH133 and clinically relevant agonists Δ^9-THC, Nabilone and ART-27.13 were included in this screen to determine the effect of mutations on potential drug treatment (**Figure 6.1**). Agonists 2-AG, CP55,940, Δ^9-THC and Nabilone were further investigated in binding affinity assays. We found that mutations in the binding pocket or structurally close to a conserved motif were detrimental for receptor activation or binding by all tested agonists. This effect was less pronounced on mutations located in the N- or C-terminus. Furthermore, activation and binding were differentially affected dependent on the combination of CB_2R mutant and agonist. Altogether, this shows the importance of precision medicine, i.e., investigating patient CB_2R genotype, prior to administration of cannabinoid-based therapies.

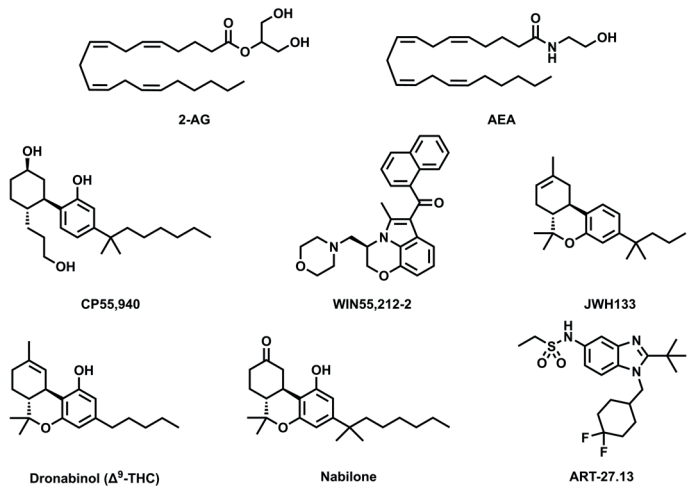

Figure 6.1 Chemical structures of cannabinoid CB_2 receptor agonists used in this study.
Endocannabinoids (2-AG and AEA), reference agonists (CP55,940, WIN55,212-2 and JWH133) and clinical agonists (Dronabinol, Nabilone and ART-27.13). CP55,940, WIN55,2121-2, Nabilone and ART-27.13 are full agonists on CB_2R, whereas 2-AG, AEA, JWH133 are partial agonist (described in **Chapter 3** and Soethoudt *et al.*)[55].

6.2 Results

6.2.1 Selection of cancer-associated CB_2R mutations

Mutations found in CB_2R in patient solid tumors were retrieved from the GDC, which resulted in a total of 85 CB_2R mutations of which 60 missense mutations. The selection was narrowed down by applying three inclusion criteria. First, nine amino acids that were mutated more than once were included. This yielded CB_2R mutations $N11^{N\text{-}term}K/S$, $D24^{N\text{-}term}N$, $E50^{1.49}D$, $R136^{3.55}H/C$, $S161^{4.53}L$, $A199^{5.48}T$, $R236^{ICL3}Q$, $A282^{7.36}T/S$ and $P348^{C\text{-}term}S/L$ (Ballesteros-Weinstein numbering in superscript). Second, presence of mutations in known conserved GPCR residues or motifs was investigated for inclusion, but no mutations were found in any of these residues or motifs. Third, mutations in the binding pocket were included. To this end, all amino acids in a 5 Å radius around the ligands, i.e., one antagonist/inverse agonist and seven agonists, in all available X-ray and cryo-EM CB_2R structures were cross-examined with the mutation list (**Figure 6.2a**). This resulted in the inclusion of five mutations $F87^{2.57}L$, $H95^{2.65}L$, $A282^{7.36}T/S$ and $L182^{ECL2}P$ in the extracellular loop 2 (ECL2) that were in close proximity to the ligand and therefore deemed part of the orthosteric binding pocket. Finally, the resulting list of mutations was compared to the natural variants reported for CB_2R in the GPCRdb, which resulted in the exclusion of six mutations ($N11^{N\text{-}}$

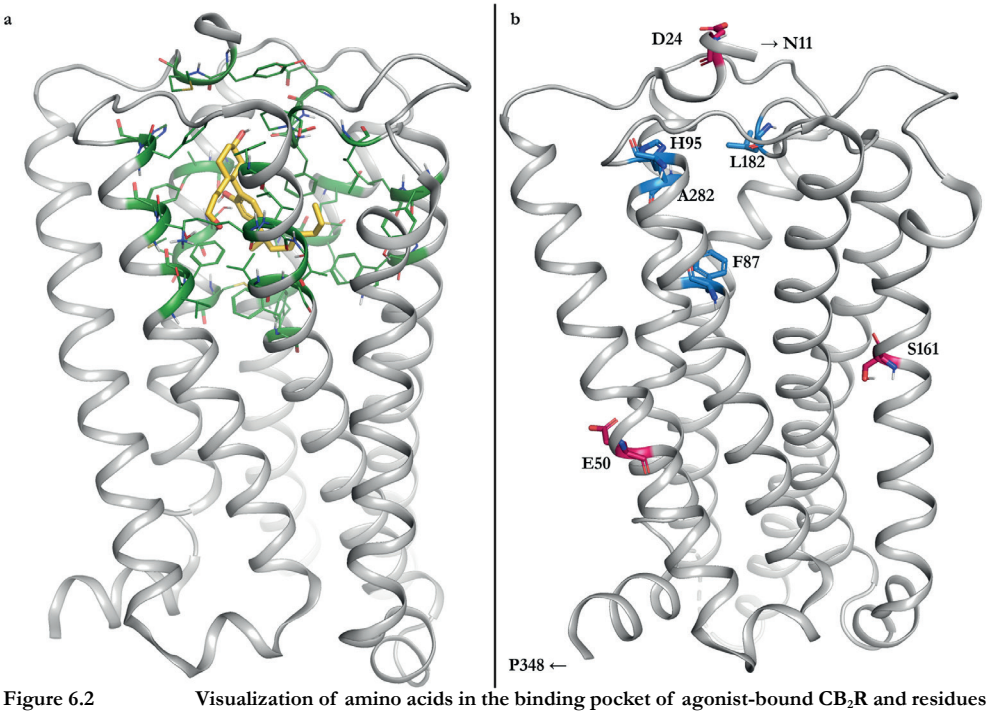

Figure 6.2 Visualization of amino acids in the binding pocket of agonist-bound CB_2R and residues bearing cancer-associated CB_2R mutations included in this study.
(a) Representative visualization of amino acids in the binding pocket of active CB_2R cryo-EM structure (8GUR) with agonist CP55,940 (yellow), showing amino acids in a 5 Å radius around the agonist (green). (b) Overview of residues investigated in this study mapped on active structure of CB_2R (8GUR). Note: Residues $N11^{N\text{-}term}$ and $P348^{C\text{-}term}$ could not be mapped, since these regions were not resolved in the structure. The colors correspond to the inclusion criteria, i.e., frequency >1 (magenta) or proximity to the orthosteric binding pocket (blue).

Table 6.1 List of selected cancer-associated mutations in CB_2R in our study identified from different cancer types.

Mutation	Primary site	Frequency	Inclusion criteria
$N11^{N\text{-}term}K$	Bronchus and lung	1	Frequency >1
$D24^{N\text{-}term}N$	Skin	2	Frequency >1
$E50^{1.49}D$	Corpus uteri, thyroid gland	2	Frequency >1
$F87^{2.57}L$	Corpus uteri	1	Binding pocket
$H95^{2.65}L$	Kidney	1	Binding pocket
$S161^{4.53}L$	Cervix uteri, bladder	2	Frequency >1
$L182^{ECL2}P$	Brain	1	Binding pocket
$A282^{7.36}T$	Corpus uteri	1	Frequency >1, binding pocket
$A282^{7.36}S$	Thyroid gland	1	Frequency >1, binding pocket
$P348^{C\text{-}term}S$	Brain, skin	2	Frequency >1

Mutations are shown in numbering of the cannabinoid CB_2 receptor (CB_2R) amino acid sequence as well as the Ballesteros-Weinstein GPCR numbering system.

^{term}S, $R136^{3.55}$H/C, $A199^{5.48}$T, $R236^{ICL3}$Q, and $P348^{C\text{-}term}$L), as they represent genetic variance and not perse a correlation to cancer. This yielded a final selection of ten mutations on nine residues due to two mutations ($A282^{7.36}$T/S) applying to two criteria (**Table 6.1**).

Seven of the nine amino acids investigated in this study were mapped on the active G protein-bound CB_2R structure with agonist CP55,940 (8GUR) (**Figure 6.2b**). Residues $N11^{N\text{-}term}$ and $P348^{C\text{-}term}$ could not be mapped on this structure, since these flexible regions were not resolved in this, or any other, CB_2R structure. Most mutations in the selected set are located in the top half of the receptor, close to the binding pocket. Mutations on $E50^{1.49}$ and $S161^{4.53}$ (and $P348^{C\text{-}term}$) are found in the bottom half of the receptor, i.e., away from the orthosteric binding pocket. Of note, the selected mutations were found in a variety of cancer types, including primary tumor sites in skin, corpus uteri and brain (**Table 6.1**).

6.2.2 Expression and receptor state of CB_2R mutants

Plasmids of all ten CB_2R mutations were generated and transiently transfected into HEK293T cells that do not endogenously express CB_2R. Wild type (WT) CB_2R was taken along as a control in all assays, which resulted in a total test set of eleven CB_2R constructs. The expression of WT and mutants CB_2R on the cell surface after transfection was examined with an ELISA and quantified as fold over mock, i.e., empty vector (**Figure 6.3a**, **Table 6.2**). The level of WT CB_2R expression was 1.6 ± 0.4 over mock and almost all mutant receptor constructs were expressed to a similar extend as WT. The expression level of mutant $D24^{N\text{-}term}N$, 2.2 ± 0.4, appeared slightly higher compared to WT, although not statistically significant. Notably, $L182^{ECL2}P$ was not expressed on the cell surface evident by a fold expression similar to mock.

To investigate whether the transiently expressed receptors were still functional, G protein activation assays were performed (**Figure 6.3b-j**, **Table 6.2**). The basal activity of all

receptor constructs was investigated and compared to WT (**Figure 6.3b**, **Table 6.2**). The basal activity of D24$^{N\text{-term}}$N was significantly increased compared to WT, whereas all other mutant receptors had a similar basal activity to WT. Potential constitutive activity of the receptors was studied by incubation with the known inverse agonist AM630 (**Figure 6.3c**, **Table 6.2**). As expected, decreased levels of activity were observed on WT which was set to -100%. D24$^{N\text{-term}}$N, the mutant with increased constitutive activity, was inhibited to a greater extent compared to WT, although not statistically significant. Activity of all other mutants was inhibited to a similar extent compared to WT (**Figure 6.3c**, **Table 6.2**). No inhibition of the constitutive activity of L182^{ECL2}P was observed, which reflected the lack of expression as determined by ELISA (**Figure 6.3a**,**c**).

Overall, most mutant receptors were expressed, and they maintained similar levels of constitutive activity compared to WT. Only mutant receptor D24$^{N\text{-term}}$N showed increased expression on the cell surface compared to WT, and also exhibited a higher level of constitutive activity.

6.2.3 Activation of CB_2R mutants by agonists

G protein activation of all CB_2R mutants was investigated for a large set of agonists with different chemotypes and partial to full agonism (**Figure 6.1**). Activation of mutant receptors was compared (and normalized) to WT activation by the specific studied agonist. To determine the physiological effect of CB_2R mutations, activation by endocannabinoids 2-AG and AEA was assessed (**Figure 6.3d**,**e**). The endocannabinoids 2-AG and AEA were able to activate D24$^{N\text{-term}}$N to a greater extent with activation levels of 144 ± 18% and 151 ± 41%, respectively, compared to their activation on WT. These activation levels corresponded to full agonism of WT CB_2R by CP55,940 (data not shown). 2-AG activation was significantly reduced on all other mutant receptors. Specifically, mutant receptors A282$^{7.36}$T and P348$^{C\text{-term}}$S were activated for 35% relative to WT, whereas all other receptors were activated less than 17% relative to WT (**Figure 6.3d**, **Table 6.2**). AEA activation on N11$^{N\text{-term}}$K, A282$^{7.36}$T and P348$^{C\text{-term}}$S was between 44% and 66% relative to WT. All other receptors were activated less than 21% by AEA (**Figure 6.3e**, **Table 6.2**).

Furthermore, activation by synthetic CB_2R agonists that have been reported in literature to attenuate cancer progression was studied, which included full agonists CP55,940 and WIN55,212-2, and partial agonist JWH133 (**Figure 6.1**, **6.3f-h**). For CP55,940, the level of activation was only similar to WT for H95$^{2.65}$L (108 ± 23%), while it was significantly decreased on mutant receptors N11$^{N\text{-term}}$K, E50$^{1.49}$D, F87$^{2.65}$L, S161$^{4.53}$L, L182^{ECL2}P, A282$^{7.36}$T, A282$^{7.36}$S and P348$^{C\text{-term}}$S and no activation was observed on mutant receptors E50$^{1.49}$D, F87$^{2.65}$L, S161$^{4.53}$L, L182^{ECL2}P (**Figure 6.3f**, **Table 6.2**). Interestingly, D24$^{N\text{-term}}$N was partially activated by CP55,940 compared to WT with a remaining 64 ± 24% activation. WIN55,212-2-mediated G protein activation was observed for all mutant CB_2R except for L182^{ECL2}P (**Figure 6.3g**, **Table 6.2**). In this case, all receptors were activated to partial levels compared to WT with activation levels between 17 ± 8% for S161$^{4.53}$L and 87 ± 7% for P348$^{C\text{-term}}$S. Finally, no JWH-133-mediated activation was observed on CB_2R mutant receptors F87$^{2.65}$L, S161$^{4.53}$L and L182^{ECL2}P and only low activation was found on E50$^{1.49}$D

(14 ± 6%) (**Figure 6.3h**, **Table 6.2**). All other mutant receptors were activated for at least 30% relative to WT yet remained partial compared to WT (**Table 6.2**).

Finally, G protein activation by the structurally diverse clinically relevant agonists Nabilone and ART-27.13 was investigated (**Figure 6.1**). No Nabilone-mediated G protein activation was observed on mutant receptors $E50^{1.49}D$, $F87^{2.57}L$ and $L182^{ECL2}P$ (**Figure 6.3i**, **Table 6.2**). Low activation of 16 ± 5% and 15 ± 11% compared to WT was found on $N11^{N\text{-}term}K$ and $S161^{4.53}L$, respectively. All other receptors were partially activated compared to WT, with activation levels between 27 ± 3% for $A282^{7.36}S$ and 81 ± 13% for $D24^{N\text{-}term}N$. ART-27.13 did not induce any G protein activation on $E50^{1.49}D$, $S161^{4.53}L$ and $L182^{ECL2}P$, while ART-27.13-mediated activation of mutant receptors $N11^{N\text{-}term}K$, $F87^{2.57}L$ and $H95^{2.65}L$ was statistically significant reduced compared to WT with activation levels of 21 ± 2 %, 17 ± 4% and 45 ± 5%, respectively, (**Figure 6.3i,j**, **Table 6.2**). $D24^{N\text{-}term}N$, $A282^{7.36}T$, $A282^{7.36}S$ and $P348^{C\text{-}term}S$ were activated at least 49% relative to WT, whereas only $A282^{7.36}T$ could be fully activated.

Screening of G protein activation by a structurally diverse set of agonists on CB_2R mutants highlighted differences between endocannabinoids, synthetic reference and clinically relevant agonists. Specifically, CB_2R receptors bearing the $H95^{2.65}L$ mutation were not activated by endocannabinoids but were partially activated by all synthetic agonists compared to WT. Mutations in N- and C-termini moderately impacted receptor activation by all agonists, whereas mutations in the binding pocket differently impacted receptor activation dependent on the agonist at hand.

6.2.4 Expression levels (B_{max}) and binding affinity (K_D) of CB_2R mutants

To investigate the binding of various agonists on the mutant receptors, binding experiments with orthosteric agonist [^{3}H]CP55,940 and inverse agonist [^{3}H]RO6957022 were performed (**Figure 6.4**). Initial binding experiments with a high concentration of membranes (20 μg membrane/well) showed that for seven mutant receptors ($E50^{1.49}D$, $F87^{2.57}L$, $H95^{2.65}L$, $S161^{4.53}L$, $L182^{ECL2}P$, $A282^{7.36}T$, $A282^{7.36}S$) low levels of [^{3}H]CP55,940 binding were detected, if any, and thus affinity of the ligands could no longer be determined on these mutant receptors (**Figure 6.4a**). However, sufficient binding of [^{3}H]CP55,940 was found for

→ Figure 6.3 Expression, receptor state and G protein activation of wild type (WT) and mutant CB_2Rs by an inverse agonist, endocannabinoids, reference and clinical agonists.
(a) Expression levels of transiently transfected WT and mutant CB_2Rs on HEK293T cells. Mock cells were transfected with empty pcDNA3.1 vector and expression data is calculated as fold over mock. Data are expressed as mean ± SD of at least two independent experiments performed in quintuplicate. (b) Basal G protein activation of WT and mutant CB_2Rs and (c) inverse agonism by 10 μM AM630. G protein activation by 10 μM of endocannabinoids (d) 2-AG and (e) AEA, 10 μM of reference agonists (f) CP55,940, (g) WIN55,212-2 and (h) JWH133, and 10 μM of clinical compounds (i) Nabilone and (j) ART-27.13. The maximum activation level of WT by the specific ligand was set to 100% while specific mutant basal activation levels were set to 0%. Data are presented as mean ± SEM of three individual experiments performed in duplicate.

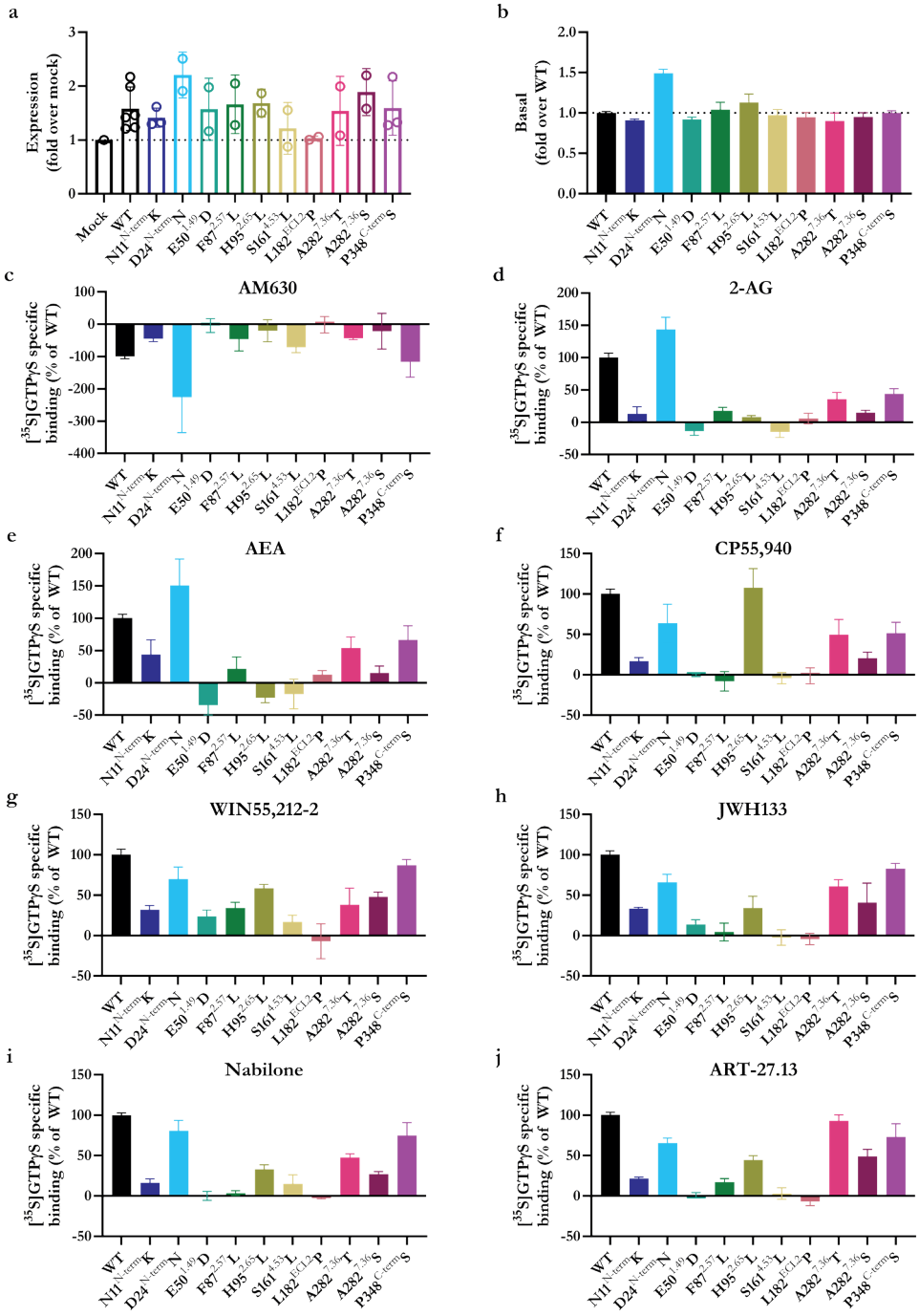
a
Expression (fold over mock)
Mock
WT
N11 N-term K
D24 N-term N
E50 1.49 D
F87 2.57 L
H95 2.65 L
S161 4.53 L
L182 ECL2 P
A282 7.36 T
A282 7.36 S
P348 C-term S
b
Basal (fold over WT)
c
AM630
[35S]GTPγS specific binding (% of WT)
d
2-AG
e
AEA
f
CP55,940
g
WIN55,212-2
h
JWH133
i
Nabilone
j
ART-27.13

Table 6.2 Expression, receptor state and G protein activation of WT and mutant CB_2Rs by 10 μM of inverse agonist, endocannabinoids, reference and clinical agonists.

Mutation	Expression (fold over mock)[a]	Basal[b] (fold over WT)	AM630[c] (%)	2-AG[c] (%)	AEA[c] (%)	CP55,940[c] (%)	WIN55,212-2[c] (%)	JWH133[c] (%)	Nabilone[c] (%)	ART-27.13[c] (%)
WT	1.6 ± 0.4	1.0 ± 0.0	-100 ± 6	100 ± 6	100 ± 5	100 ± 5	100 ± 6	100 ± 3	100 ± 3	100 ± 3
N11$^{N\text{-term}}$K	1.4 ± 0.2	0.9 ± 0.0	-45 ± 9	13 ± 11*	44 ± 22	17 ± 5*	32 ± 5*	33 ± 2*	16 ± 5*	21 ± 2*
D24$^{N\text{-term}}$N	2.2 ± 0.4	1.5 ± 0.1*	-226 ± 110	144 ± 18*	151 ± 41	64 ± 24	70 ± 15	66 ± 10	81 ± 13*	65 ± 6
E50$^{1.49}$D	1.6 ± 0.6	0.9 ± 0.0	-4 ± 22	-14 ± 6*	-34 ± 21*	0 ± 2*	24 ± 8*	14 ± 6*	0 ± 6*	1 ± 3*
F87$^{2.57}$L	1.7 ± 0.5	1.0 ± 0.1	-46 ± 36	17 ± 6*	21 ± 18*	-8 ± 12*	34 ± 7*	4 ± 11*	3 ± 3*	17 ± 4*
H95$^{2.65}$L	1.7 ± 0.3	1.1 ± 0.1	-20 ± 34	8 ± 2*	-23 ± 8*	108 ± 23	59 ± 5	34 ± 14*	33 ± 6*	45 ± 5*
S161$^{4.53}$L	1.2 ± 0.5	1.0 ± 0.1	-72 ± 16	-15 ± 9*	-17 ± 23*	-4 ± 7*	17 ± 8*	-2 ± 10*	15 ± 11*	3 ± 7*
L182^{ECL2}P	1.0 ± 0.0	0.9 ± 0.1	-2 ± 25	6 ± 8*	13 ± 6*	-1 ± 10*	-7 ± 22*	-4 ± 7*	-3 ± 1*	-7 ± 5*
A282$^{7.36}$T	1.5 ± 0.6	0.9 ± 0.1	-44 ± 4	36 ± 10*	54 ± 17	49 ± 19*	38 ± 20*	61 ± 8*	47 ± 5	93 ± 8
A282$^{7.36}$S	1.9 ± 0.4	0.9 ± 0.1	-22 ± 55	15 ± 4*	15 ± 11*	21 ± 7*	48 ± 6*	41 ± 24*	27 ± 3*	49 ± 9
P348$^{C\text{-term}}$S	1.6 ± 0.5	1.0 ± 0.0	-116 ± 48	44 ± 8*	66 ± 22	51 ± 14*	87 ± 7	83 ± 6	75 ± 16*	73 ± 16

Mutations are shown in numbering of the cannabinoid CB_2 receptor (CB_2R) amino acid sequence as well as the Ballesteros-Weinstein GPCR numbering system. [a] Expression level of WT and mutant CB_2Rs are presented as fold over mock (empty pcDNA3.1 vector) and are mean ± SD of at least two individual experiments performed in quintuplicate. [b] Basal activity expressed as fold change over WT in [^{35}S]GTPγS assays. [c] Percentage of G protein activation by 10 μM compound compared to WT. Values are mean ± SEM of three independent experiments performed in duplicate. One-way ANOVA with Dunnett's posthoc test was used to analyze differences in activation compared to WT (*$p < 0.05$).

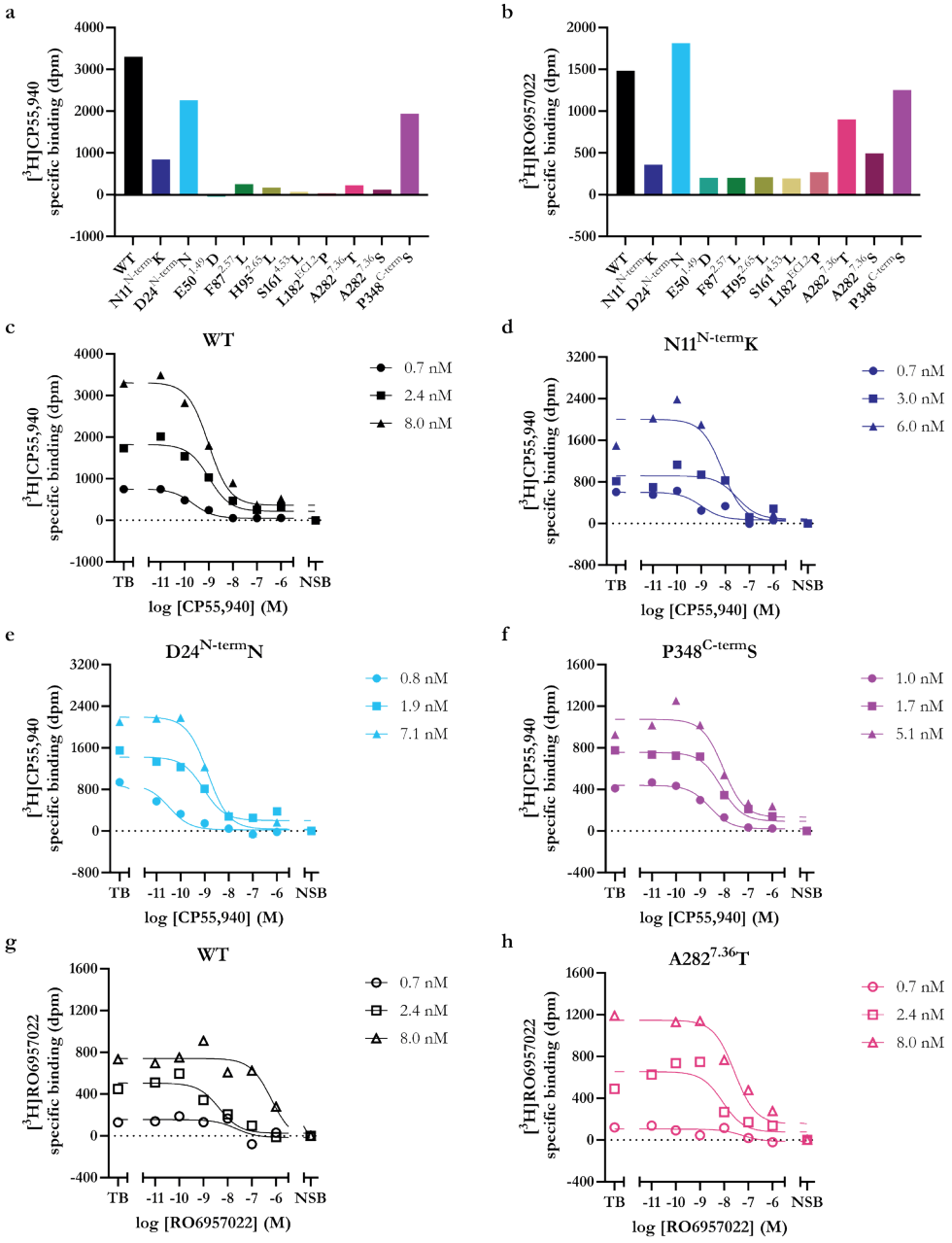

Figure 6.4 Specific binding of agonist [^{3}H]CP55,940 and inverse agonist [^{3}H]RO6957022 on WT and mutant CB_2Rs.

Specific binding of (a) agonist [^{3}H]CP55,940 and (b) inverse agonist [^{3}H]RO6957022 to membranes expressing WT or mutant CB_2R (20 µg/well). Homologous displacement experiment with (c) WT, (d) N11$^{N\text{-term}}$K, (e) D24$^{N\text{-term}}$N and (f) P348$^{C\text{-term}}$S CB_2R using [^{3}H]CP55,940. Homologous displacement experiments with (g) WT and (h) A282$^{7.36}$T CB_2R using [^{3}H]RO6957022. Total binding (TB) of the radioligand is set to 100% and non-specific binding (NSB) of radioligand was determined the presence of cold ligand and set to 0%. Data shown are specific radioligand binding of a representative experiment of at least two (a, b) or three (c-h) experiments performed in duplicate.

mutant receptors $N11^{N\text{-}term}K$, $D24^{N\text{-}term}N$ and $P348^{C\text{-}term}S$, which were further characterized in homologous displacement assays. Similarly, all mutant receptors were screened at the same high membrane concentration in [^{3}H]RO6957022 binding assays (**Figure 6.4b**). This resulted in low levels of [^{3}H]RO6957022 binding for seven mutant receptors ($N11^{N\text{-}term}K$, $E50^{1.49}D$, $F87^{2.57}L$, $H95^{2.65}L$, $S161^{4.53}L$, $L182^{ECL2}P$, $A282^{7.36}S$). Similar to the screen with [^{3}H]CP55,940, sufficient binding of [^{3}H]RO6957022 was found for mutant receptors $D24^{N\text{-}term}N$ and $P348^{C\text{-}term}S$. However, sufficient binding of the radioligand was also found on $A282^{7.36}S$ with this radioligand. Therefore, binding to this mutant was further characterized in [^{3}H]RO6957022 binding assays.

Homologous displacements with CP55,940 on WT, $N11^{N\text{-}term}K$, $D24^{N\text{-}term}N$ and $P348^{C\text{-}term}S$ yielded affinities of CP55,940 on these mutants similar to WT with pK_D values between 8.4 ± 0.2 and 8.8 ± 0.1 (**Figure 6.4c-f**, **Table 6.3**). Likewise, the affinity of inverse agonist RO6957022 on CB_2R was not statistically significant impacted by the $A282^{7.36}T$ mutation (**Figure 6.4g**,**h**, **Table 6.3**). Homologous displacement experiments with CP55,940 and RO6957022 also yielded B_{max} values for receptor expression in the membranes used. B_{max} values were slightly reduced for $N11^{N\text{-}term}K$ and $D24^{N\text{-}term}N$ compared to WT, whereas it was significantly reduced for $P348^{C\text{-}term}S$ to 1.0 ± 0.2 compared to 2.3 ± 0.5 for WT (**Table 6.3**). The expression level of $A282^{7.36}T$ was 2-fold higher than on WT, but not statistically significant different (**Table 6.3**).

Altogether, binding of both radioligands [^{3}H]CP55,940 and [^{3}H]RO6957022 was negatively impacted for six mutant receptors $E50^{1.49}D$, $F87^{2.57}L$, $H95^{2.65}L$, $S161^{4.53}L$, $L182^{ECL2}P$ and $A282^{7.36}S$. Nevertheless, binding of [^{3}H]CP55,940 could still be detected on $N11^{N\text{-}term}K$, $D24^{N\text{-}term}N$ and $P348^{C\text{-}term}S$, while sufficient binding of [^{3}H]RO6957022 was observed on mutant receptors $D24^{N\text{-}term}N$, $A282^{7.36}T$ and $P348^{C\text{-}term}S$. The affinity of CP55,940 for $N11^{N\text{-}term}K$, $D24^{N\text{-}term}N$ and $P348^{C\text{-}term}S$ and RO6957022 for $A282^{7.36}T$ was not significantly altered compared to WT and expression levels were similar to WT, except for $P348^{C\text{-}term}S$ which was reduced.

6.2.5 Binding affinity of reference agonists at CB_2R mutants

Binding affinity at $N11^{N\text{-}term}K$, $D24^{N\text{-}term}N$, $A282^{7.36}T$ and $P348^{C\text{-}term}S$, i.e., the mutants that still showed sufficient binding, was investigated for a selection of agonists. Since endocannabinoids 2-AG and AEA behaved similarly on all mutant receptors in G protein activation assays, only 2-AG was selected for further profiling (**Figure 6.3d**,**e**, **6.5a,b**). Similarly, affinity of only Nabilone was examined as activation by Nabilone and ART-27.13 was similarly impacted by all mutant receptors (**Figure 6.3i,j**). This was supplemented with affinity determination of clinical agonist Δ^9-THC, which did not yield detectable G protein activation levels (**Chapter 3**). The affinity of 2-AG was significantly, yet moderately, increased on mutant receptors $D24^{N\text{-}term}N$ and $P348^{C\text{-}term}S$ to 5.8 ± 0.1 and 5.6 ± 0.1, respectively, compared to 5.1 ± 0.1 on WT (**Figure 6.5a**, **Table 6.3**). Mutation $N11^{N\text{-}term}K$ did not influence the binding affinity of 2-AG on CB_2R. The affinity of 2-AG on mutant CB_2R $A282^{7.36}T$, as detected in [^{3}H]RO6957022 binding assays, was slightly, yet significantly reduced compared to WT with pK_i values of 5.6 ± 0.1 and 6.1 ± 0.1, respectively (**Figure**

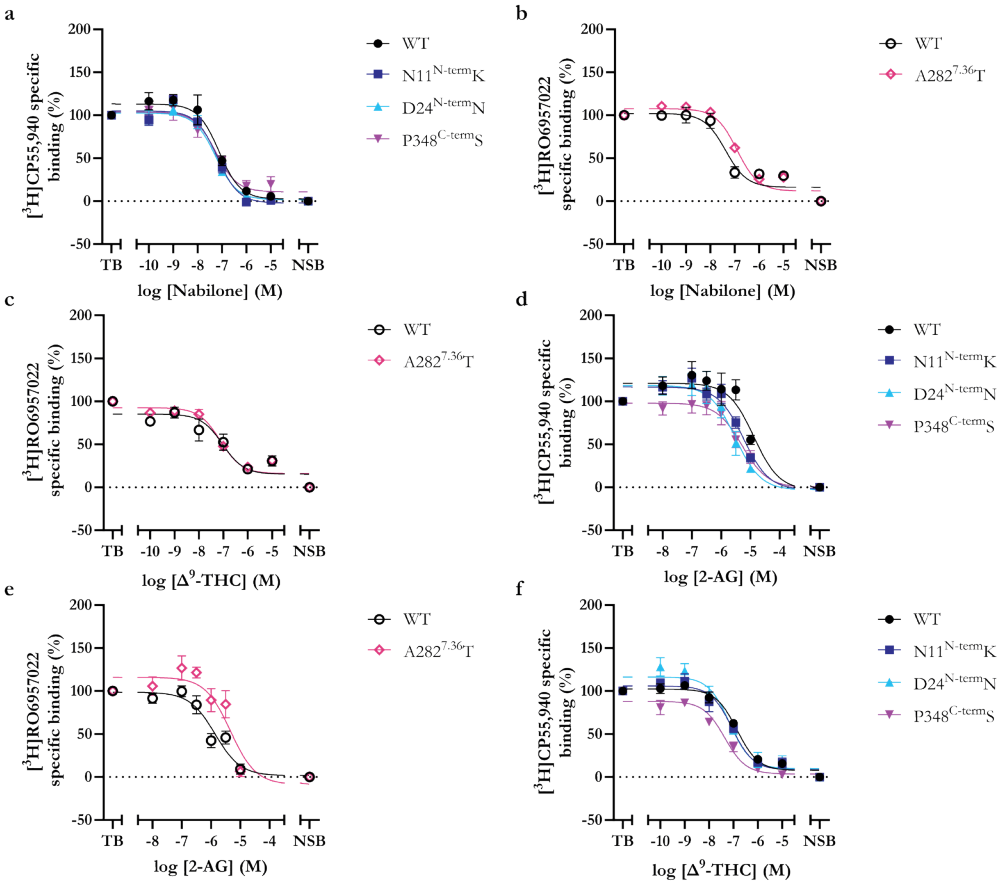

Figure 6.5 Affinity of endogenous agonist and clinical agonists on WT and mutant CB_2Rs.
Displacement of [^{3}H]CP55,940 (WT, N11$^{N\text{-term}}$K, D24$^{N\text{-term}}$N and P348$^{C\text{-term}}$S) or [^{3}H]RO6957022 (WT and A282$^{7.36}$T) with (a,b) endogenous agonist 2-AG, and (c,d) clinical agonists Δ^9-THC and (e,f) Nabilone. Total binding (TB) of the radioligand is set to 100% and non-specific binding (NSB) of radioligand was determined the presence of cold ligand and set to 0%. Data are the mean ± SEM of at least three experiments performed in duplicate.

6.5b, **Table 6.3**). Furthermore, the binding affinity of Δ^9-THC and Nabilone was not affected by mutations N11$^{N\text{-term}}$K, D24$^{N\text{-term}}$N or P348$^{C\text{-term}}$S (**Figure 6.5c**,**e**, **Table 6.3**). Similarly, the affinity of Δ^9-THC was not affected on A282$^{7.36}$T (**Figure 6.5d**, **Table 6.3**). However, binding affinity of Nabilone was significantly reduced to 7.1 ± 0.1 on A282$^{7.36}$T compared to 7.6 ± 0.1 for WT (**Figure 6.5f**, **Table 6.3**). In conclusion, the impact of the investigated CB_2R mutations on binding affinity of reference agonists 2-AG, Δ^9-THC and Nabilone was agonist-dependent, and if any, only moderate effects were observed.

6.2.6 Structural mapping of cancer-associated CB_2R mutations

Most of the mutations in the CB_2R binding pocket negatively affected the activation or binding by agonists. Strikingly, mutant H95$^{2.65}$L responded differently to the endocannabinoids

Table 6.3 Expression levels (B_{max}) and affinities of CP55,940, RO6957022, 2-AG, Δ^9-THC and Nabilone for WT and mutant CB_2R determined from radioligand binding assays.

	[^{3}H]CP55,940 binding assays			[^{3}H]RO6957022 binding assays		
Mutation	**B_{max} (pmol/mg)**	**pK_D (K_D (nM))**		**B_{max} (pmol/mg)**	**pK_D (K_D (nM))**	
WT	2.3 ± 0.5	8.6 ± 0.0 (2.6)		0.5 ± 0.0	8.8 ± 0.1 (1.5)	
N11$^{N\text{-term}}$K	1.1 ± 0.2	8.4 ± 0.2 (4.1)		N.A.	N.A.	
D24$^{N\text{-term}}$N	1.9 ± 0.3	8.8 ± 0.1 (1.7)		N.A.	N.A.	
A282$^{7.36}$T	N.A.	N.A.		1.0 ± 0.2	8.8 ± 0.2 (1.7)	
P348$^{C\text{-term}}$S	1.0 ± 0.2*	8.8 ± 0.1 (1.7)		N.A.	N.A.	
	pK_i 2-AG	**pK_i Δ^9-THC**	**pK_i Nabilone**	**pK_i 2-AG**	**pK_i Δ^9-THC**	**pK_i Nabilone**
WT	5.1 ± 0.1	7.1 ± 0.1	7.4 ± 0.1	6.1 ± 0.1	7.2 ± 0.4	7.6 ± 0.1
N11$^{N\text{-term}}$K	5.4 ± 0.0	7.3 ± 0.2	7.3 ± 0.1	N.A.	N.A.	N.A.
D24$^{N\text{-term}}$N	5.8 ± 0.1***	7.5 ± 0.1	7.5 ± 0.2	N.A.	N.A.	N.A.
A282$^{7.36}$T	N.A.	N.A.	N.A.	5.6 ± 0.1†	7.4 ± 0.2	7.1 ± 0.1††
P348$^{C\text{-term}}$S	5.6 ± 0.1**	7.6 ± 0.1	7.6 ± 0.1	N.A.	N.A.	N.A.

Values are mean ± SEM of three independent experiments performed in duplicate. No affinity and expression values were determined for mutants E50$^{1.49}$D, F87$^{2.57}$L, H95$^{2.65}$L, S161$^{4.53}$L, L182^{ECL2}P, A282$^{7.36}$S due to no or too low levels of specific radioligand binding. One-way ANOVA with Dunnett's multiple comparisons test or an unpaired t-test was performed to analyzed differences in pK_D, B_{max} or pK_i values compared to WT ($^{*}p<0.05$, $^{**}p<0.01$, $^{***}p<0.001$ in [^{3}H] CP55,940 assays or $^{\dagger}p<0.05$, $^{\dagger\dagger}p<0.01$ in [^{3}H]RO6957022 assays).

compared to synthetic agonists, i.e., activation by 2-AG and AEA was completely abolished compared to WT, while partial activation remained for all synthetic agonists (**Figure 6.3**, **Table 6.2**). Further structural investigation of this residue demonstrated that H95$^{2.65}$ is in close proximity to the cyclohexanol group of CP55,940 (5.7 Å) and as such might interact with agonists (**Figure 6.6a**).

Furthermore, differences in activation levels of the A282$^{7.36}$T and A282$^{7.36}$S CB_2Rs, i.e., receptors with two different mutations on the same residue, were observed and these also differently impacted affinity of inverse agonist RO6957022 (**Figure 6.3**, **6.4**). From the cryo-EM structure with CP55,940, it can be observed that the carbonyl of this residue is located near the agonist and the hydroxyl on the phenol core of CP55,940 (4.4 Å) (**Figure 6.6a**). The cyclohexanol group of CP55,940 is moved away from the methyl group at a distance of 6.4-6.7 Å.

Finally, mutation E50$^{1.49}$D significantly impacted receptor activation by all agonists and the binding of [^{3}H]CP55,940 and [^{3}H]RO69557022 was greatly reduced, while the expression level remained similar to WT (**Figure 6.3**, **6.4**). Closer examination of this residue in the cryo-EM structure indicated that E50$^{1.49}$ is structurally close to P296$^{7.50}$ in the conserved NPxxY motif (4.4 Å), which might aid in the stabilization of the receptor (**Figure 6.6b**). As such, reduction of the amino acid side chain by the E50$^{1.49}$D mutation might destabilize the receptor and alter its function.

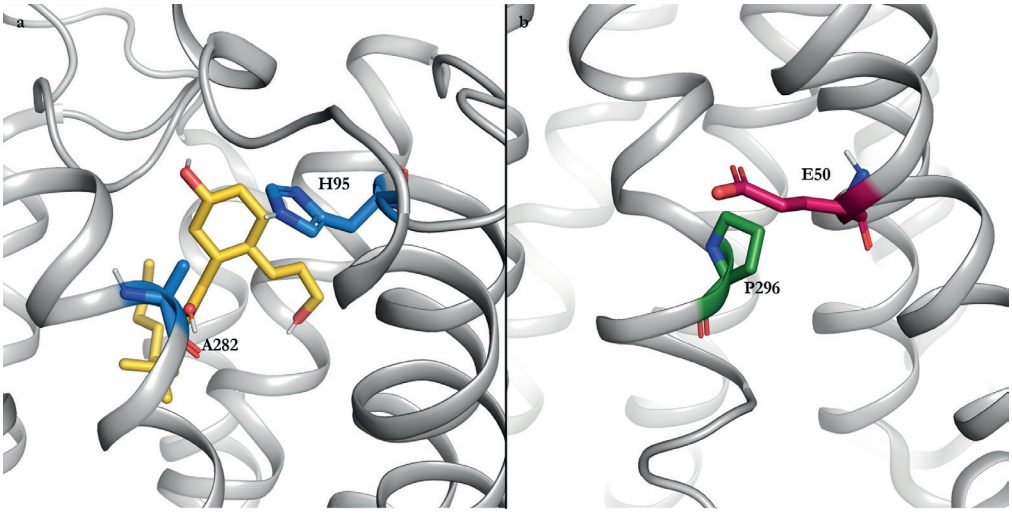

Figure 6.6 Structural visualization of residues H95$^{2.65}$, A282$^{7.36}$ and E50$^{1.49}$ in CB_2R structure with agonist CP55,940.
Overview of specific residues investigated in this study mapped on active structure of CB_2R (grey; 8GUR). (a) Zoom in on binding pocket with CP55,940 (yellow) and residues H95$^{2.65}$ and A282$^{7.36}$ (blue). (b) Zoom in on residue E50$^{1.49}$ (magenta) and structurally close NPxxY motif residue P296$^{7.50}$ (green).

6.3 Discussion

Cancer is the second leading cause of death globally and research to more efficacious and safer therapies is constantly ongoing[31]. Recently, the role of GPCRs in cancer development and progression is becoming more acknowledged since GPCR-mediated cell signaling pathways have been associated with cell migration, survival, and growth[5]. As such a small number of GPCR drugs and antibodies are in clinical trials as cancer therapies[6]. Various *in vitro* and *in vivo* studies on different cancer types have also specifically shown the beneficial effects of CB_2R activation[22–25]. Nevertheless, in 20% of all cancers GPCRs are mutated, which might interfere with endogenous signaling or targeting of these receptors[2,3,7–11]. In this chapter, we investigated the impact of cancer-associated CB_2R mutations on endogenous binding and activation, as well as the druggability of these mutant receptors by a variety of CB_2R agonists.

Mutations in CB_2R were extracted from the GDC and narrowed down to include the most frequently mutated locations as well as mutations in vicinity to the binding pocket (**Figure 6.2**, **Table 6.1**). The resulting ten mutations were transiently transfected into HEK293T cells (**Figure 6.3a**, **Table 6.2**). Of these, only CB_2R with the L182^{ECL2}P mutation was not expressed on the cell membrane and as such no responses were observed in functional or binding assays (**Figure 6.3**, **6.4**, **Table 6.2**). We, in **Chapter 4**, and others previously showed that L182^{ECL2} is involved in binding of diverse agonists since a mutation to isoleucine (L182^{ECL2}I) reduced the potency of agonists but not expression of the receptor[32–35]. Nevertheless, mutations to or from proline (P) are more often described to have a detrimental effect on receptor activity and trafficking to the cell membrane as the rigid backbone of proline provokes a forced turn in the protein sequence[9,36]. The swap to

proline in the ECL2, and close to the binding pocket, thus most likely interferes with the trafficking of the receptor to the cell membrane and as such is detrimental. This suggests that patients bearing the CB_2R $L182^{ECL2}P$ mutation will no longer benefit from endogenous protection or respond to cannabinoid-based therapies.

On the other hand, the exchange of proline for serine (S) in the C-terminus ($P348^{C\text{-}term}S$), distant from the binding pocket, did not prevent receptor trafficking to the cell membrane, but significantly reduced the expression level of this mutant receptor in binding assays (**Figure 6.3a**, **Table 6.2**, **6.3**). Furthermore, we observed reduced G protein activation levels by this mutant receptor for various agonists compared to WT (**Figure 6.3d-j**, **Table 6.2**). The swap from proline to serine introduces an extra site on the C-terminus for a post-translational modifications (PTM), which are involved in control of the dynamics of signaling[37,38]. Specifically, serine residues, opposed to proline, on the C-terminus are prone to phosphorylation, which might initiate the recruitment of ß-arrestins and desensitization or internalization of the receptor[37,38]. Similarly, PTMs on the N-terminus of GPCRs have been described to be involved in the receptor folding, trafficking and regulation of binding and signaling[37,38]. Asparagines (N) are prone to *N*-glycosylation and specifically, CB_2R $N11^{N\text{-}term}$ was described to be glycosylated in mammalian cell lines, which contributed to a higher protein stability[39]. As such, the reduced agonist-mediated G protein activation on CB_2R mutant $N11^{N\text{-}term}K$ might be due to losing a glycosylation site (**Figure 6.3**, **Table 6.2**)[40]. In contrast, the increased basal activity and levels of G protein activation of mutant receptor $D24^{N\text{-}term}N$ might be attributed to the gain of a glycosylation site (**Figure 6.3b**,**c**, **Table 6.2**).

In **Chapter 4** and other studies, hydrophobic interactions in the orthosteric pocket of CB_2R between $F87^{2.57}$ and/or $H95^{2.65}$ and various (inverse) agonists are described[32,33,35]. Interestingly, CP55,940-mediated inhibition of cAMP accumulation was investigated on CB_2R $F87^{2.57}A$ and $H95^{2.65}A$ mutants, which revealed a decrease in agonist potency with a small or no effect on its efficacy[33]. This contrasts with the loss of or reduced G protein activation by CP55,940 and other agonists in our studies on $F87^{2.57}L$ and $H95^{2.65}L$ (**Figure 6.3**, **Table 6.2**). Pathway amplification by measurement of downstream second messengers, such as cAMP, might explain these contrasting results[41]. Furthermore, $H95^{2.65}$ has been postulated to maintain a polar network with $S285^{7.39}$ around orthosteric ligands, which might be disturbed in our studies by switching to hydrophobic leucine (L) (**Figure 6.6a**). Interestingly, the endocannabinoids were not able to activate $H95^{2.65}L$ CB_2R, whereas synthetic agonists still activated the receptor albeit partially (**Figure 6.3**). Different functional effects of endocannabinoids compared to synthetic agonists were previously also reported by Hillger *et al.* on lymphoblastoid cell lines (LCLs) from individuals with different CB_2R genotypes[42]. This emphasizes the importance of including various chemotypes to explore the effects of disease-associated mutations on receptor behavior.

One amino acid in the patient data set was mutated twice, namely $A282^{7.36}$, which was located close to the binding pocket (**Figure 6.6a**). Although structurally-related, we found profound differences between the $A282^{7.36}T$ and $A282^{7.36}S$ mutations. Consistently higher activation by the different agonists on the $A282^{7.36}T$ mutant was found compared to $A282^{7.36}S$ (**Figure 6.3**, **Table 6.2**). Furthermore, in binding studies only CB_2R $A282^{7.36}T$ could be bound by an inverse agonist, whereas binding to $A282^{7.36}S$ could not be quantified

(**Figure 6.4**, **6.5**, **Table 6.3**). Hydrophobic interactions between A282$^{7.36}$ and HU308 have been postulated in **Chapter 4**, which may be disturbed by the polar residues serine and threonine (T) in our studies[32]. Furthermore, this specific residue has previously been described to shape the ligand entry pathway to the CB_2R orthosteric pocket and a mutation towards phenylalanine (F) occluded the entry pathway for JWH133[43]. We hypothesize that the two studied mutations might also interfere with the shaping of the ligand entry pathway. However, the differences between the two mutants requires more experimental validation. Nevertheless, it becomes evident that mutations near the orthosteric binding pocket have a substantial impact on the physiological function and druggability of CB_2R.

Mutations E50$^{1.49}$D and S161$^{4.53}$L were structurally distant from the binding pocket, yet they significantly affected G protein activation and binding of agonists to the receptors (**Figure 6.3**, **6.4a**,**b**, **Table 6.2**). Two independent cancer genome analysis studies revealed a high mutational frequency amongst GPCRs of residues at position 1.49 and 4.53[3,4]. A key role for tight packing of transmembrane helices is attributed to S$^{4.53}$ in several class A GPCRs and mutations to leucine have been shown to disrupt the structure or activation patterns of these receptors[10,44,45]. Furthermore, in the ß$_2$-adrenoceptor residue 1.49 appeared to be structurally proximal to the conserved NPxxY motif, which is involved in receptor folding, localization and regulation of signaling[4]. Upon closer examination of this region in the CB_2R active cryo-EM structure from **Chapter 4** (8GUR), we observed that NPxxY residue P296$^{7.50}$ was structurally close to E50$^{1.49}$ (**Figure 6.6b**)[32]. This suggests that the specific orientations of E50$^{1.49}$ and S161$^{4.53}$ are important for the structural stability and functionality of CB_2R and reduction of the amino acid side chain by the E50$^{1.49}$D mutation might destabilize and alter receptor function.

It should be noted that conclusions from this study are based on functional screening results. Therefore, the functional investigation of these mutations should be expanded to determine the potency of different agonists. As such, the [^{35}S]GTPγS assays that were used in this screen could be continued or a switch to another G protein-dependent assay could be made. However, it may be of interest to also include ß-arrestin-2 recruitment assays since we hypothesize that PTMs may differ on the P348$^{C\text{-term}}$S mutation compared to WT and consequently could alter ß-arrestin-2 recruitment. Furthermore, to investigate whether mutations introduce or remove PTMs, SDS-page and mass spectrometry-based quantitative proteomic experiments might be executed on mutant receptors N11$^{N\text{-term}}$K, D24$^{N\text{-term}}$N and P348$^{C\text{-term}}$S[38,48]. The recently developed a multiplex assay to simultaneously investigate the inhibition of cAMP production and ß-arrestin-2 recruitment (**Chapter 3**) may serve as a platform to screen functional responses of mutant receptors. This assay can be easily adapted to transiently express CB_2R mutants, opposed to the ß-arrestin-2 recruitment assay in **Chapter 2**, and investigate simultaneously their effect on two different pathways. The kinetic context in this assay might highlight further kinetic differences between the mutants, which was previously shown for A_{2A} receptor mutation that affected a ligand's dissociation[46]. Moreover, most mutations caused a decrease in sensitivity to agonist stimulation, which may aid the tumor cells to evade the antitumor effects of CB_2R activation. As such these mutations might be driver mutations, but more research is required to examine whether they are actually driver or passenger mutations[47]. Ultimately, experiments focusing on cancer processes, such as migration and proliferation, might be executed with CB_2R mutants to

investigate the impact on cancer development and progression. These experiments could be extended to cancer relevant cell lines making use of the CRISPR-Cas9 technology[49,50].

In conclusion, our results indicate that cancer-associated mutations in CB_2R can impact the expression, agonist binding and activation of the receptor. Binding of agonists and subsequent activation of CB_2R was reduced or completely abolished for CB_2Rs with mutations in the binding pocket. Unexpectedly, mutations distant from the binding pocket also affected the receptor behavior most likely by interfering with conserved motifs or transmembrane packaging. Ultimately, mutations in the N- and C-terminus altered the CB_2R expression levels possibly due to the introduction or removal of post-translational modifications. Interestingly, there might be differences between the activation of the mutant receptors by endogenous and synthetic agonists as we found clear differences on specifically the $H95^{2.65}L$ mutant. Altogether, this study emphasizes the importance of personalized medicine by examination of the patient's genetic composition of CB_2R prior to treatment with cannabinoid-based therapeutics. Follow-up experimentation is required to further investigate the implications of the selected cancer-associated CB_2R mutations on cancer development and progression. Furthermore, the mutant selection can be expanded to include more mutations from the GDC to obtain a broad understanding of targeting CB_2R in cancer.

6.4 Materials and methods

6.4.1 Chemicals and reagents

Primary rabbit anti-HA tag polyclonal antibody was obtained from ThermoFisher (Waltham, MA, USA) and secondary goat anti-rabbit HRP-conjugated antibody was from Jackson ImmunoResearch (Cambridgeshire, UK). Compounds 2-arachidonoylglycerol (2-AG), anandamide (AEA), WIN55,212-2, JWH133 and phenylmethylsulfonyl fluoride (PMSF) were bought from Tocris Bioscience (Bristol, UK). CP55,940 was obtained from Sigma-Aldrich (St. Louis, MO, USA), while Nabilone and ART-27.13 were provided by F. Hoffmann-La Roche Ltd (Basel, Switzerland). RO6957022 and [^{3}H]RO6957022 (specific activity 82.8 Ci/mmol) were custom-synthesized and custom-labeled, respectively, by F. Hoffmann-La Roche Ltd. [^{3}H]CP55,940 (specific activity 108.5 Ci/mmol), guanosine 5'-O-[γ-thio]triphosphate ([^{35}S]GTPγS, specific activity 1250 Ci/mmol) and GF/C filter plates were purchased from PerkinElmer (Waltham, MA, USA). Bicinchoninic acid (BCA) and BCA protein assay reagent were purchased from Pierce Chemical Company (Rockford, IL, USA). All other chemicals were of analytical grade and obtained from standard commercial sources. Buffers and solutions were prepared at room temperature (rt) using Millipore water (deionized using a MilliQ A10 Biocel™, with a 0.22 μm filter).

6.4.2 Data mining and mutation selection

Cancer-associated mutations in CB_2R were retrieved from Genomic Data Commons (GDC) (version 21.0). A selection of missense mutations was made based on a mutation frequency

>1 or mutation towards two different amino acids. Furthermore, structural importance was investigated by inclusion of mutations in conserved GPCR regions (x.50, Ballesteros-Weinstein numbering) or motifs (DRY, CWxP, NPxxY), and mutations in the orthosteric binding pocket. The orthosteric binding pocket residues were defined in all eight CB_2R X-ray or cryo-EM structures (6KPC, 6KPF, 6PT0, 5ZTY, 8GUQ, 8GUR, 8GUS, 8GUT) by direct interactions of the ligand with amino acids or amino acids in a 5 Å radius around the ligand. The respective receptor structures were retrieved from the Protein Data Bank (PDB) using the fetch function in PyMOL Molecular Graphics System version 2.4 (Schrödinger, LLC., NY, USA) and hydrogen atoms were added. Using built-in functionality, the selection of the ligand was expanded to all residues around it within 5 Å. All mutations that were reported as natural variants in the GPCRdb (release Oct. 25, 2019) were excluded from our study[51].

6.4.3 Plasmid design and isolation

Primers were designed using the QuikChange® Primer Design feature from Agilent Technologies (Santa Clara, CA, USA) and ordered via Integrated DNA Technologies (Coralville, IA, USA). An N-terminal 3×HA-tagged human wild type cannabinoid CB_2 receptor (WT hCB_2R) (cDNA Resource Center; Bloomsburg, PA, USA) cloned into pcDNA3.1(+) was used as a template for mutations. Mutations were generated with the QuikChange II Site-Directed Mutagenesis Kit (Agilent Technologies) according to the protocol. In short, 50 ng of the template was mixed with 10 µM forward and reverse primer, 1 µL of deoxyribonucleotide triphosphate (dNTP) mix, 2.5 µL of 10× reaction buffer and 2.5 U *PfuUltra* HF DNA polymerase in a total volume of 20 µL. The PCR reaction was performed in a T100™ Thermal Cycler (Biorad; Irvine, CA, USA) for 22 cycles consisting of 30 s at 98 °C, 1 min at 55 °C and 10 min at 68 °C. The template DNA was then removed by incubating the mixture with 5 U of *Dpn I* restriction enzyme for 2 h at 37 °C before transforming the plasmids into XL-1 Blue supercompetent cells according to the kit's protocol. The plasmids were isolated with the QIAprep mini and midi plasmid purification kits (Qiagen; Germantown, MD, USA). All mutations were confirmed by double-strain DNA sequencing (Leiden Genome Technology Center; Leiden, the Netherlands).

6.4.4 Cell culture, transfection, and membrane preparation

Human embryonic kidney 293 T (HEK293T) cells were grown as monolayers in culture medium i.e., Dulbecco's Modified Eagle's Medium, supplemented with 10% fetal calf serum, 2 mM L-glutamine, 100 IU/mL penicillin and 100 µg/mL streptomycin under a humidified atmosphere at 37 °C with 5% CO_2. Subculture was done twice a week at 80 – 90% confluence on 10 cm ø plates by trypsinization.

HEK293T were transfected with WT or mutant hCB_2R as previously described in **Chapter 4**[32]. In short, cells were seeded on 10 cm ø plates 24 h prior to transfection to reach approximately 50% confluence at the start of transfection. The cells were transfected with 10 µg plasmid DNA of WT or mutant hCB_2R using the calcium phosphate precipitation

method. To this end, a DNA-calcium mix was made containing 270 mM $CaCl_2$ and 10 μg plasmid DNA to which Hank's Balanced Salt Solution (HBSS; 280 mM NaCl, 10 mM KCl, 1.5 mM Na_2HPO_4 and 50 mM HEPES) was added in a 1:1 (v/v) ratio and mixed by aeration to create consistent calcium phosphate precipitates. For transfection, 1 mL DNA-calcium mix was added per 10 cm ø plate, followed by a 48 h incubation under a humidified atmosphere at 37 °C with 5% CO_2.

For membrane preparation, transient HEK293T cells were harvested 48 h after transfection. Cells were detached by scraping into 3 mL of PBS and subsequently centrifuged at 2000 × g for 5 min. Pellets were resuspended in ice-cold Tris buffer (50 mM Tris-HCl, pH 7.4) and homogenized with an Ultra Turrax homogenizer (IKA-Werke GmbH & Co. KG; Staufen, Germany). Cytosolic and membrane fractions were separated using a high-speed centrifugation step of 31,000 rpm (100,000 × g) in a Beckman Optima LE-80K ultracentrifuge with Ti70 Rotor for 20 min at 4 °C. After a second cycle of homogenization and centrifugation, the final pellets were resuspended in 50 mM Tris-HCl (pH 7.4) and stored in 100 μL aliquots at -80 °C until use. Membrane protein concentrations were determined using a BCA protein determination assay as described by the manufacturer[52].

6.4.5 ELISA

Receptor expression after transfection was measured in an enzyme-linked immunosorbent assay (ELISA). After 24 h of transfection, HEK293T cells were detached with PBS/EDTA and seeded into a sterile 96-well poly-D-lysine coated plate at a density of 100,000 cells per well. After an additional 24 h incubation under a humidified atmosphere at 37 °C with 5% CO_2, cells were washed with PBS and fixed with 4% formaldehyde for 10 min at rt. Cells were washed twice with tris-buffered saline (TBS) and were blocked with TBS supplemented with 0.1% TWEEN 20 (TBST) and 2% BSA (w/v) for 1 h at rt while shaking. Subsequently, the cells were incubated with rabbit anti-HA tag polyclonal antibody (1:2500) for 1 h at rt while shaking. After removal of the antibody, the cells were washed three times with TBST and incubated with the secondary goat anti-rabbit HRP-conjugated antibody (1:6000) for 30 min at rt while shaking. After a final wash with TBS, the cells were treated with 3,3',5,5'-tetramethylbenzidine (TMB) in the dark for maximally 10 min at rt to visualize immunoreactivity. The reaction was quenched with 1 M H_3PO_4, and absorbance was read at 450 nm with a Wallac EnVision 2104 Multilabel reader (Revvity; Waltham, MA, USA).

6.4.6 [^{35}S]GTPγS binding assays

G protein activation by agonists 2-AG, AEA, CP55,940, WIN55,212-2, JWH133, Nabilone, ART-27.13 and inverse agonist AM630 was measured by binding of radiolabeled [^{35}S] GTPγS to WT and mutant CB_2R as previously described in **Chapter 4**[32]. In short, transiently transfected HEK293T membrane homogenates (10 μg/well) were diluted in assay buffer (50 mM Tris-HCl (pH 7.4), 5 mM $MgCl_2$, 150 mM NaCl, 1 mM EDTA, 0.05% BSA (w/v) and 1 mM DTT, freshly prepared every day) and were pretreated with 10 μg saponin and 1 μM GDP for 30 minutes at rt. For endocannabinoid samples, the membranes were additionally

preincubated with 50 μM PMSF before agonist addition. To determine G protein activation, the membranes were incubated with 10 μM agonist and [^{35}S]GTPγS (0.3 nM) for 90 minutes at 25 °C while shaking at 400 rpm. Basal receptor activity was determined in the presence of vehicle (i.e., acetonitrile for endocannabinoids, and DMSO for all other compounds). Incubations were terminated by rapid vacuum filtration with ice-cold 50 mM Tris-HCl (pH 7.4) and 5 mM $MgCl_2$ wash buffer through Whatman GF/C filters using a Filtermate 96-well harvester (Revvity). Filters were dried for at least 30 min at 55 °C and subsequently 25 μL MicroScint scintillation cocktail was added per well. Filter-bound radioactivity was measured by scintillation spectrometry using a Microbeta^2 2450 counter (Revvity).

6.4.7 [^{3}H]CP55,940 binding assays

Agonist affinity (K_D, K_i) on WT and mutant CB_2R ($N11^{N\text{-term}}K$, $D24^{N\text{-term}}N$, $P348^{C\text{-term}}S$) was determined in [^{3}H]CP55,940 displacement assays. The amount of transiently transfected HEK293T membranes ranged from 2.5 μg to 20 μg protein per well, i.e., optimized to obtain a specific [^{3}H]CP55,940 binding window of ~1000 disintegrations per minute (dpm). Membranes were thawed and subsequently homogenized using the Ultra Turrax homogenizer. For experiments with endocannabinoids, the membranes were preincubated for 30 min with 50 μM PMSF. Homologous displacement assays were performed with three concentrations of [^{3}H]CP55,940 of ~0.7 nM, ~1.5 nM and ~7.0 nM in the presence of competing CP55,940 (ranging from 0.01 nM to 1 μM) in assay buffer (50 mM Tris-HCl (pH 7.4), 5 mM $MgCl_2$, 0.1% BSA (w/v)). Heterologous displacement assays were performed using ~1.5 nM final concentration of [^{3}H]CP55,940 with six increasing concentrations of 2-AG, Δ^9-THC and Nabilone (ranging from 0.1 nM to 10 μM) in assay buffer. In both assays, binding was initiated by addition of membrane homogenates to reach a final volume of 100 μL. Non-specific binding (NSB) was determined using 10 μM CP55,940. Organic solvent, i.e., acetonitrile for 2-AG, and DMSO for all other compounds, concentrations were <1% in all samples. Total binding (TB) did not exceed 10% of the amount added to prevent ligand depletion. Incubation was done for 2 h at 25 °C to reach equilibrium. Filtration was performed and filter-bound radioactivity was determined as described in section **6.4.6 [^{35}S] GTPγS binding assays** except for using ice-cold 50 mM Tris-HCl (pH 7.4), 5 mM $MgCl_2$, 0.1% BSA (w/v) as wash buffer.

6.4.8 [^{3}H]RO6957022 binding assays

Agonist affinity (K_D, K_i) on WT and mutant CB_2R ($A282^{7.36}T$) was determined in [^{3}H] RO6957022 displacement assays as described in **Chapter 5**[53]. The amount of transiently transfected HEK293T membranes ranged from 9 μg to 20 μg protein per well, i.e., optimized to obtain a specific [^{3}H]RO6957022 binding window of ~1000 dpm. Membranes were thawed and subsequently homogenized using the Ultra Turrax homogenizer. For experiments with endocannabinoids, the membranes were preincubated for 30 min with 50 μM PMSF. Incubations were performed at 10 °C. Therefore, assay buffer, (radio)ligands and membranes were precooled to 10 °C prior to the experiment. Homologous displacement

assays were performed with three concentrations of [^{3}H]RO6957022 of ~0.7 nM, ~2.4 nM and ~8.0 nM in the presence of competing RO6957022 (ranging from 0.01 nM to 1 μM) in assay buffer (50 mM Tris-HCl (pH 7.4), 0.1% BSA (w/v)). Heterologous displacement assays were executed using ~1.5 nM final concentration [^{3}H]RO6957022 with six increasing concentrations of 2-AG, Δ^9-THC and Nabilone (ranging from 0.1 nM to 10 μM) in assay buffer. For both assays, binding was initiated by addition of membrane homogenates to reach a final volume of 100 μL. NSB was determined using 10 μM RO6957022. Organic solvent, i.e., acetonitrile for 2-AG, and DMSO for all other compounds, concentrations were <1% in all samples. TB did not exceed 10% of the amount added to prevent ligand depletion. Incubation was done for 2 h at 10 °C to reach equilibrium. Filtration was performed and filter-bound radioactivity was determined as described in **6.4.6 [^{35}S]GTPγS binding assays** except for using ice-cold 50 mM Tris-HCl (pH 7.4), 0.1% BSA (w/v) as wash buffer.

6.4.9 Structural mapping

Figures were created based on the experimentally determined cryo-EM structure of G protein-bound CB_2R with agonist CP55,940 in **Chapter 4** (PDB: 8GUR)[32]. Figures were generated using PyMOL Molecular Graphics System version 2.4.

6.4.10 Data analysis and statistics

All experimental data were analyzed using GraphPad Prism 9.0 (GraphPad Software Inc.; San Diego, CA, USA). All values obtained are means ± standard error of the mean (SEM) of at least three independent experiments performed in duplicate, unless stated otherwise.

[^{35}S]GTPγS agonist responses on hCB_2R constructs were baseline-corrected for the individual mutant's basal activity and the responses were normalized to the basal activity of the specific construct (0%) and maximal activation on WT (100%). Basal activity was represented as fold over WT.

Displacement assays were baseline-corrected with NSB and normalized to this value (0%) and TB (100%). The equilibrium dissociation constants (K_D) of [^{3}H]CP55,940 or [^{3}H]RO6957022 on different mutants were calculated from homologous displacements by non-linear regression analysis, using the "one-site homologous" model. The half-maximal inhibitory concentrations (pIC_{50}) of the agonists in [^{3}H]CP55,940 and [^{3}H]RO6957022 assays were obtained by non-linear regression analysis of the heterologous displacement curves and further converted into inhibitory constant pK_i using the Cheng-Prusoff equation[54]. For this conversion, the experimentally determined K_D for each construct in [^{3}H]CP55,940 or [^{3}H]RO6957022 assays was used.

Differences in activation, pK_D and pK_i values for each mutant compared to WT were analyzed using a one-way ANOVA with Dunnett's multiple comparisons test or an unpaired t-test. Significant differences in activation are displayed as * $p< 0.05$ and differences in affinity are displayed as * $p < 0.05$; ** $p < 0.01$, *** $p < 0.001$ and **** $p < 0.0001$.

6.5 Acknowledgements

We thank Mea Abani, Jenny Lam, Lynn H. Somsen and Yasmine S.O. Jamani for their experimental support.

References

1. Hanahan, D. Hallmarks of Cancer: New Dimensions. *Cancer Discov* **12**, 31–46 (2022).
2. O'Hayre, M. *et al.* The Emerging Mutational Landscape of G-proteins and G-protein Coupled Receptors in Cancer. *Nat Rev Cancer* **13**, 424 (2013).
3. Bongers, B. J. *et al.* Pan-cancer functional analysis of somatic mutations in G protein-coupled receptors. *Sci Rep* **12**, 1–15 (2022).
4. Huh, E. *et al.* Recurrent high-impact mutations at cognate structural positions in class A G protein-coupled receptors expressed in tumors. *Proc Natl Acad Sci U S A* **118**, (2021).
5. Chaudhary, P. K. & Kim, S. An Insight into GPCR and G-Proteins as Cancer Drivers. *Cells* **10**, 3288 (2021).
6. Usman, S., Khawer, M., Rafique, S., Naz, Z. & Saleem, K. The current status of anti-GPCR drugs against different cancers. *J Pharm Anal* **10**, 517–521 (2020).
7. Wang, X. *et al.* Cancer-Related Somatic Mutations in Transmembrane Helices Alter Adenosine A1 Receptor Pharmacology. *Molecules* **27**, 3742 (2022).
8. Wang, X. *et al.* Cancer-related somatic mutations alter adenosine A1 receptor pharmacology - A focus on mutations in the loops and C-terminus. *The FASEB Journal* **36**, e22358 (2022).
9. den Hollander, L. S. *et al.* Impact of cancer-associated mutations in CC chemokine receptor 2 on receptor function and antagonism. *Biochem Pharmacol* **208**, 115399 (2023).
10. Feng, C. *et al.* Cancer-Associated Mutations of the Adenosine A_{2A} Receptor Have Diverse Influences on Ligand Binding and Receptor Functions. *Molecules* **27**, 4676 (2022).
11. Wang, X. *et al.* Characterization of cancer-related somatic mutations in the adenosine A2B receptor. *Eur J Pharmacol* **880**, 173126 (2020).
12. Howlett, A. C. & Abood, M. E. CB_1 and CB_2 Receptor Pharmacology. in *Advances in Pharmacology* vol. 80 169–206 (Academic Press, 2017).
13. Brennecke, B. *et al.* Cannabinoid receptor type 2 ligands: An analysis of granted patents since 2010. *Pharm Pat Anal* **10**, 111–163 (2021).
14. Pertwee, R. G. *et al.* International Union of Basic and Clinical Pharmacology. LXXIX. Cannabinoid Receptors and Their Ligands: Beyond CB_1 and CB_2. *Pharmacol Rev* **62**, 588–631 (2010). Fraguas-Sánchez, A. I., Martín-Sabroso, C. & Torres-Suárez, A. I. Insights into the effects of the endocannabinoid system in cancer: a review. *Br J Pharmacol* **175**, 2566–2580 (2018).
15. Pagano, C., Navarra, G., Coppola, L., Bifulco, M. & Laezza, C. Molecular mechanism of cannabinoids in cancer progression. *Int J Mol Sci* **22**, (2021).
16. Pérez-Gómez, E. *et al.* Role of Cannabinoid Receptor CB_2 in HER2 Pro-oncogenic Signaling in Breast Cancer. *J Natl Cancer Inst* **107**, 77 (2015).
17. Sánchez, C. *et al.* Inhibition of Glioma Growth in Vivo by Selective Activation of the CB_2 Cannabinoid Receptor. *Cancer Res* **61**, 5784–5789 (2001).
18. Blasco-Benito, S. *et al.* Therapeutic targeting of HER2–CB_2R heteromers in HER2-positive breast cancer. *Proc Natl Acad Sci U S A* **116**, 3863–3872 (2019).
19. Xu, S., Ma, H., Bo, Y. & Shao, M. The oncogenic role of CB2 in the progression of non-small-cell lung cancer. *Biomedicine & Pharmacotherapy* **117**, 109080 (2019).
20. Iden, J. A. *et al.* The Anti-Tumorigenic Role of Cannabinoid Receptor 2 in Colon Cancer: A Study in Mice and Humans. *Int J Mol Sci* **24**, (2023).
21. Hinz, B. & Ramer, R. Anti-tumour actions of cannabinoids. *Br J Pharmacol* **176**, 1384–1394 (2019).
22. Mangal, N. *et al.* Cannabinoids in the landscape of cancer. *J Cancer Res Clin Oncol* **147**, 2507–2534 (2021).
23. Ladin, D. A., Soliman, E., Griffin, L. T. & Van Dross, R. Preclinical and clinical assessment of cannabinoids as anti-cancer agents. *Front Pharmacol* **7**, 361 (2016).
24. Hashiesh, H. M., Sharma, C., Goyal, S. N., Jha, N. K. & Ojha, S. Pharmacological Properties, Therapeutic Potential and Molecular Mechanisms of JWH133, a CB2 Receptor-Selective Agonist. *Front Pharmacol* **12**, 1818 (2021).
25. Blázquez, C. *et al.* Cannabinoids inhibit glioma cell invasion by down-regulating matrix metalloproteinase-2 expression. *Cancer Res* **68**, 1945–1952 (2008).
26. Qamri, Z. *et al.* Synthetic cannabinoid receptor agonists inhibit tumor growth and metastasis of breast cancer. *Mol Cancer Ther* **8**, 3117–3129 (2009).
27. Casanova, M. L. *et al.* Inhibition of skin tumor growth and angiogenesis in vivo by activation of cannabinoid receptors. *Journal of Clinical Investigation* **111**, 43–50 (2003).

28. Bhaskaran, D. *et al.* A randomised phase II trial of temozolomide with or without cannabinoids in patients with recurrent glioblastoma (ARISTOCRAT): protocol for a multi-centre, double-blind, placebo-controlled trial. *BMC Cancer* **24**, 83 (2024).

29. Rock, E. M. & Parker, L. A. Cannabinoids As Potential Treatment for Chemotherapy-Induced Nausea and Vomiting. *Front Pharmacol* **7**, (2016).

30. Wild, C. P., Weiderpass, E. & Stewart. B.W. *World Cancer Report: Cancer Research for Cancer Prevention*. (International Agency for Research on Cancer, Lyon, France, 2020).

31. Li, X. *et al.* Structural basis of selective cannabinoid CB_2 receptor activation. *Nat Commun* **14**, 1–16 (2023). **(Chapter 4)**

32. Li, X. *et al.* Crystal Structure of the Human Cannabinoid Receptor CB2. *Cell* **176**, 459–467 (2019).

33. Hua, T. *et al.* Activation and Signaling Mechanism Revealed by Cannabinoid Receptor-G_i Complex Structures. *Cell* **180**, 655-665.e18 (2020).

34. Xing, C. *et al.* Cryo-EM Structure of the Human Cannabinoid Receptor CB2-G_i Signaling Complex. *Cell* **180**, 645-654.e13 (2020).

35. Ulloa-Aguirre, A., Zariñán, T., Dias, J. A. & Conn, P. M. Mutations in G protein-coupled receptors that impact receptor trafficking and reproductive function. *Mol Cell Endocrinol* **382**, 411–423 (2014).

36. Zhang, B., Li, S. & Shui, W. Post-Translational Modifications of G Protein-Coupled Receptors Revealed by Proteomics and Structural Biology. *Front Chem* **10**, (2022).

37. Patwardhan, A., Cheng, N. & Trejo, J. Post-Translational Modifications of G Protein–Coupled Receptors Control Cellular Signaling Dynamics in Space and Time. *Pharmacol Rev* **73**, 120–151 (2021).

38. Yeliseev, A. *et al.* Thermostability of a recombinant G protein-coupled receptor expressed at high level in mammalian cell culture. *Sci Rep* **10**, 16805 (2020).

39. Cabral, G. A. & Griffin-Thomas, L. T. Emerging role of the cannabinoid receptor CB_2 in immune regulation: Therapeutic prospects for neuroinflammation. *Expert Rev Mol Med* **11**, (2009).

40. Kolb, P. *et al.* Community guidelines for GPCR ligand bias: IUPHAR review 32. *Br J Pharmacol* **179**, 3651–3674 (2022).

41. Hillger, J. M. *et al.* Phenotypic screening of cannabinoid receptor 2 ligands shows different sensitivity to genotype. *Biochem Pharmacol* **130**, 60–70 (2017).

42. Casajuana-Martin, N. *et al.* A Single Point Mutation Blocks the Entrance of Ligands to the Cannabinoid CB_2 Receptor via the Lipid Bilayer. *J Chem Inf Model* **62**, 5771–5779 (2022).

43. Sanchez-Reyes, O. B. *et al.* G Protein-Coupled Receptors Contain Two Conserved Packing Clusters. *Biophys J* **112**, 2315–2326 (2017).

44. Chelikani, P. *et al.* Role of group-conserved residues in the helical core of β_2-adrenergic receptor. *Proc Natl Acad Sci U S A* **104**, 7027–7032 (2007).

45. Guo, D. *et al.* Molecular basis of ligand dissociation from the adenosine A_{2A} receptor. *Mol Pharmacol* **89**, 485–491 (2016).

46. Arang, N. & Gutkind, J. S. G Protein-Coupled receptors and heterotrimeric G proteins as cancer drivers. *FEBS Lett* **594**, 4201–4232 (2020).

47. Soethoudt, M. *et al.* Selective Photoaffinity Probe That Enables Assessment of Cannabinoid CB_2 Receptor Expression and Ligand Engagement in Human Cells. *J Am Chem Soc* **140**, 6067–6075 (2018).

48. Ng, S. K. *et al.* The protective effect of cannabinoids against colorectal cancer cachexia through modulation of inflammation and immune responses. *Biomedicine and Pharmacotherapy* **161**, (2023).

49. Chen, G. & Obal, D. Detecting and measuring of GPCR signaling – comparison of human induced pluripotent stem cells and immortal cell lines. *Front Endocrinol (Lausanne)* **14**, (2023).

50. Pándy-Szekeres, G. *et al.* GPCRdb in 2018: Adding GPCR structure models and ligands. *Nucleic Acids Res* **46**, D440–D446 (2018).

51. Smith, P. K. *et al.* Measurement of protein using bicinchoninic acid. *Anal Biochem* **150**, 76–85 (1985).

52. Bouma, J. *et al.* Dual allosteric and orthosteric pharmacology of synthetic analog cannabidiol-dimethylheptyl, but not cannabidiol, on the cannabinoid CB_2 receptor. *Biochem Pharmacol* **218**, 115924 (2023). **(Chapter 5)**

53. Cheng, Y.-C. & Prusoff, W. H. Relationship between the inhibition constant (K1) and the concentration of inhibitor which causes 50 per cent inhibition (I50) of an enzymatic reaction. *Biochem Pharmacol* **22**, 3099–3108 (1973).

54. Soethoudt, M. *et al.* Cannabinoid CB_2 receptor ligand profiling reveals biased signalling and off-target activity. *Nat Commun* **8**, 1–14 (2017).